INTERNATIONAL JOURNAL FOR NUMERICAL METHODS IN FLUIDS
Int. J. Numer. Meth. Fluids 2007; **54**:453–471
Published online 19 December 2006 in Wiley InterScience (www.interscience.wiley.com). DOI: 10.1002/fld.1410

Semi-Lagrangian semi-implicit time-splitting scheme for the shallow water equations

A. Bourchtein*, † and L. Bourchtein

Institute of Physics and Mathematics, Pelotas State University, Brazil

SUMMARY

Time-splitting technique applied in the context of the semi-Lagrangian semi-implicit method allows the use of extended time steps mainly based on physical considerations and reduces the number of numerical operations at each time step such that it is approximately proportional to the number of the points of spatial grid. To control time growth of the additional truncation errors, the standard stabilizing correction method is modified with no penalty for accuracy and efficiency of the algorithm. A linear analysis shows that constructed scheme is stable for time steps up to 2 h. Numerical integrations with actual atmospheric fields of pressure and wind confirm computational efficiency, extended stability and accuracy of the proposed scheme. Copyright © 2006 John Wiley & Sons, Ltd.

Received 13 April 2006; Revised 25 October 2006; Accepted 25 October 2006

KEY WORDS: semi-Lagrangian method; time splitting; shallow water equations

1. INTRODUCTION

The shallow water (SW) equations are frequently used for modelling the hydrodynamics of coastal oceans, lakes and estuaries, simulation of flows in channels and rivers, study of large-scale waves and height-averaged regimes in the atmosphere and ocean and so on. During the initial years of the numerical weather prediction (in the 1950s–1960s) they were successfully used for forecasting the middle troposphere dynamics and later (in the 1960s–1970s) for the study of general circulation of atmosphere.

However, in our view, it is most important that these equations keep essential properties of more complete 3D systems (Navier–Stokes, Euler and hydrostatic equations). First, they contain

*Correspondence to: A. Bourchtein, Rua Anchieta 4715 bloco K, ap.304, Pelotas 96020-250, Brazil.
†E-mail: burstein@terra.com.br

Contract/grant sponsor: Brazilian science foundation CNPq

both nonlinear gravity and advective terms, imposing hard computational penalty on fully implicit methods. Second, linearized form of these equations supports secondary fast waves and principal slow waves, giving rise to problems associated with stiff equations. Also, the SW equations maintain the mathematical type of more complex systems: the inviscid form of the SW equations is of hyperbolic type (just like 3D Euler equations), inclusion of viscosity in the momentum equations leads to incompletely parabolic system (such as 3D Navier–Stokes equations) and a set of the linearized SW equations with different mean heights is equivalent to linearized 3D hydrostatic equations used as the primitive system in the majority of the models of geophysical fluid dynamics. Besides, such characteristics as the presence of a set of equations and variety of unknown functions allow to check important characteristics of numerical schemes on different space and time grids. All these properties make SW equations an important testing system for computational fluid dynamics, especially for atmosphere and ocean modelling. Indeed, it has become customary, in developing new numerical methods for weather prediction or oceanography, to study first the SW equations.

In the last two decades, the semi-implicit semi-Lagrangian method became one of the most efficient and popular techniques for numerical solution of the differential equations of atmosphere dynamics. It allows to overcome the Courant–Friedrichs–Lewy (CFL) condition with respect to both gravity and inertial waves at the low cost of solving a set of trajectory equations and linear elliptic problems at each time step. In semi-Lagrangian methods, the CFL condition is usually substituted by the Pudykiewicz–Benoit–Staniforth condition, which guarantees the convergence of iterations for trajectory equations and is a rather weak restriction: the maximum allowable time step is inversely proportional to the modulus of wind gradient, which allows to choose time steps on the base of accuracy considerations [1, 2]. Semi-Lagrangian semi-implicit methods are currently used in the majority of research and operational atmospheric models [3–10], and have started to be considered for oceanographic simulations [11–13].

To circumvent the remaining computationally expensive problem of solution of elliptic equations, different time-splitting techniques have been applied in the context of the atmospheric models [14–18]. Splitting methods allow decoupling of multidimensional elliptic equations into a set of 1D problems, which are solved very efficiently by direct Thomas algorithm. Unfortunately, to the best of our knowledge, all reports on application of the splitting techniques in atmospheric models indicate the fast growth of the splitting truncation error when the time step exceeds the CFL advection criterion [14, 16–18]. To reduce the splitting errors, Douglas *et al.* have recently proposed small modifications to the splitting method in the case of parabolic equations [19, 20]. In this study, we apply the last technique to the semi-Lagrangian semi-implicit stabilizing correction (SC) scheme for the SW equations, analyse stability and accuracy properties of the obtained scheme, describe respective computational algorithm and present the results of numerical tests. Let us note that although directional splitting methods require the use of the rectangular computational domains, it is not any critical restriction for atmospheric problems, because the majority of atmospheric models are designed on rectangular domains. Of course, it can be an essential restriction for some oceanographic problems related to physical domains with curvilinear boundaries. However, consideration of this matter is out of scope of our study.

The outline of the paper is as follows. In Section 2, we describe the design of a single time step of the semi-Lagrangian semi-implicit SC scheme applied to the SW equations. In Section 3, we analyse the accuracy and stability properties of the algorithm, in particular, splitting technique and its modification. The results of numerical experiments with actual atmospheric data are presented in Section 4.

DOI: 10.1002/fld

2. DESIGN OF ONE TIME STEP OF THE NUMERICAL ALGORITHM

2.1. Primitive equations and spatial discretization

In the rotated reference system, 2D inviscid SW equations can be written in the form [21, 22]

$$\partial_t \mathbf{W} = (\mathbf{A}_x + \mathbf{G}_x)\,\partial_x \mathbf{W} + \left(\mathbf{A}_y + \mathbf{G}_y\right)\partial_y \mathbf{W} + \mathbf{C}\mathbf{W} \tag{1}$$

where x, y are the Cartesian spatial coordinates, t is the time coordinate, $\mathbf{W} = (u, v, \Phi)^{\mathrm{T}}$ is unknown vector function whose entries are the velocity components u and v, and the geopotential $\Phi = gz$ with gravitational acceleration g and height z, $f = 2\Omega \sin\phi$ is the Coriolis parameter, Ω is the modulus of angular velocity of the Earth's rotation. The matrices

$$\mathbf{A}_x = \begin{pmatrix} u & 0 & 0 \\ 0 & u & 0 \\ 0 & 0 & u \end{pmatrix}, \quad \mathbf{A}_y = \begin{pmatrix} v & 0 & 0 \\ 0 & v & 0 \\ 0 & 0 & v \end{pmatrix}, \quad \mathbf{G}_x = \begin{pmatrix} 0 & 0 & 1 \\ 0 & 0 & 0 \\ \Phi & 0 & 0 \end{pmatrix}$$

$$\mathbf{G}_y = \begin{pmatrix} 0 & 0 & 0 \\ 0 & 0 & 1 \\ 0 & \Phi & 0 \end{pmatrix}, \quad \mathbf{C} = \begin{pmatrix} 0 & -f & 0 \\ f & 0 & 0 \\ 0 & 0 & 0 \end{pmatrix}$$

represent contribution of advection, gravitational and Coriolis forces.

We use the spatial staggered uniform grid E with mesh size h (see Figure 1), which assures better dispersion relations than grid A and allows to avoid excessive interpolations inherent in grid C [23–25]. The points allocated for velocity components have subscript V and the geopotential points are marked by Φ.

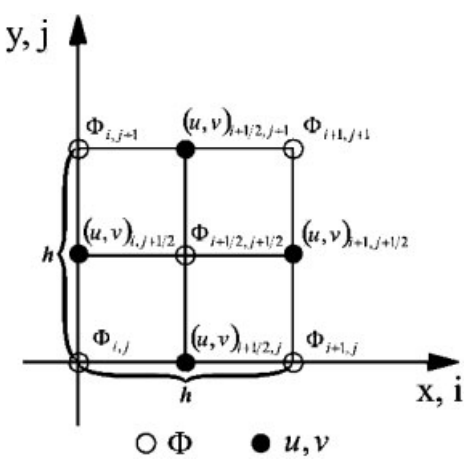

Figure 1. The staggered E grid.

DOI: 10.1002/fld

All spatial operators are approximated with the second order of accuracy. In particular, the following central differences are used for respective derivatives at the points $V_{i,j+1/2}$ and $\Phi_{i+1/2,j+1/2}$:

$$\delta_{xV}\Phi = \frac{\Phi_{i+1/2,j+1/2} - \Phi_{i-1/2,j+1/2}}{h}, \quad \delta_{yV}\Phi = \frac{\Phi_{i,j+1} - \Phi_{i,j}}{h}$$

$$\delta_{x\Phi}u = \frac{u_{i+1,j+1/2} - u_{i,j+1/2}}{h}, \quad \delta_{y\Phi}v = \frac{v_{i+1/2,j+1} - v_{i+1/2,j}}{h}$$

In time we use fixed time step τ defined on the base of accuracy and stability considerations. Considering that all unknown functions are found for time levels $t_0, \ldots, t_n (t_j = j\tau)$, we describe in this section the algorithm of computation of unknowns at time level $t_n + 1$.

2.2. *Solution of the advective part*

At the first stage the advective part of equations

$$\partial_t \mathbf{W} = \mathbf{A}_x \partial_x \mathbf{W} + \mathbf{A}_y \partial_y \mathbf{W} \tag{2}$$

is solved by using the method of characteristics. Each of Equations (2) can be written as

$$\partial_t \phi = u\partial_x \phi + v\partial_y \phi, \quad \phi = u, v, \Phi$$

representing passive or self-induced advection. Therefore, characteristics equations for all three equations in (2) have the form

$$d_t \mathbf{X} = \mathbf{V}(t, \mathbf{X}), \quad \mathbf{X} = (x, y), \quad \mathbf{V} = (u, v)$$

The last equations are approximated in time with the second-order accuracy

$$\frac{\mathbf{X}^{n+1} - \mathbf{X}^n}{\tau} = \mathbf{V}^{n+1/2}\left(\frac{\mathbf{X}^{n+1} + \mathbf{X}^n}{2}\right) \tag{3}$$

where the velocity components are extrapolated to the intermediate time level with the second order of accuracy

$$\mathbf{V}^{n+1/2} = \tfrac{1}{2}(3\mathbf{V}^n - \mathbf{V}^{n-1}) \tag{4}$$

or the third order of accuracy

$$\mathbf{V}^{n+1/2} = \tfrac{1}{8}(15\mathbf{V}^n - 10\mathbf{V}^{n-1} + 3\mathbf{V}^{n-2}) \tag{5}$$

Additional 'initial' conditions for (3) are the final positions of trajectories on the time interval $[t_n, t_{n+1}]$.

Considered on the E grid, Equations (3) are completed by the final positions (the arrival points) assigned to grid points

$$\mathbf{X}^{n+1} = \mathbf{X}_{Vi,j+1/2}$$

and solved for the initial positions (the departure points) related to V-points. The velocity components at the middle points used in (3) are calculated by bi-linear interpolation. The initial positions for Φ-points are found by bi-linear interpolation using four closest V-points.

DOI: 10.1002/fld

This algorithm was studied and applied by different authors employing semi-Lagrangian approach. It assures the second order of accuracy, and a sufficient condition for convergence of the fixed point iterations has the form

$$\tau \leqslant \frac{1}{\max(|\partial_x u|, |\partial_y u|, |\partial_x v|, |\partial_y v|)} \tag{6}$$

[5, 8, 1, 26, 2, 27]. Substituting characteristic values of the velocity fields at the middle troposphere in (6), one can find that the maximum allowable time step is about 110 min.

2.3. Gravity wave solution

Now we treat the gravity and Coriolis terms

$$\partial_t \mathbf{W} = \mathbf{G}_x \partial_x \mathbf{W} + \mathbf{G}_y \partial_y \mathbf{W} + \mathbf{C}\mathbf{W} \tag{7}$$

According to semi-Lagrangian approach, these terms are approximated along the trajectories found at the advective stage. We apply SC scheme with additional terms, which help to control the values of the splitting errors:

$$\begin{aligned}
&\frac{u^{n+1,1}-u^n}{\tau} = f v^n - \delta_{xV}\Phi^n \\
&\qquad -\alpha\left[\frac{\tau f^2}{4}(u^n - u^{n-1}) + \frac{\tau f}{4}\delta_{yV}(\Phi^n - \Phi^{n-1}) - \frac{\tau\Phi_0}{4}\delta_{xV}\delta_{y\Phi}(v^n - v^{n-1})\right] \\
&\frac{v^{n+1,1}-v^n}{\tau} = -f u^n - \delta_{yV}\Phi^n, \quad \frac{\Phi^{n+1,1}-\Phi^n}{\tau} = -\Phi^n(\delta_{x\Phi}u^n + \delta_{y\Phi}v^n)
\end{aligned} \tag{8}$$

$$\begin{aligned}
&\frac{u^{n+1,2}-u^{n+1,1}}{\tau} = f\frac{v^{n+1,2}-v^n}{2} - \delta_{xV}\frac{\Phi^{n+1,2}-\Phi^n}{2}, \quad \frac{v^{n+1,2}-v^{n+1,1}}{\tau} = 0 \\
&\frac{\Phi^{n+1,2}-\Phi^{n+1,1}}{\tau} = -\Phi_0\delta_{x\Phi}\frac{u^{n+1,2}-u^n}{2}
\end{aligned} \tag{9}$$

$$\begin{aligned}
&\frac{u^{n+1}-u^{n+1,2}}{\tau} = 0, \quad \frac{v^{n+1}-v^{n+1,2}}{\tau} = -f\frac{u^{n+1}-u^n}{2} - \delta_{yV}\frac{\Phi^{n+1}-\Phi^n}{2} \\
&\frac{\Phi^{n+1}-\Phi^{n+1,2}}{\tau} = -\Phi_0\delta_{y\Phi}\frac{v^{n+1}-v^n}{2}
\end{aligned} \tag{10}$$

Here, ϕ^{n-1}, ϕ^n and ϕ^{n+1}, $\phi = u, v, \Phi$ denote the principal values of unknown functions at the 'past' t_{n-1}, 'current' t_n and 'future' t_{n+1} time levels, respectively, and $\phi^{n+1,1}$ and $\phi^{n+1,2}$ denote the intermediate (temporary) values, assigned to the arrival points at the time level t_{n+1}. The constant Φ_0 in the third equations of (9) and (10) is the mean value of the geopotential. The values at each departure point are found by bi-cubic interpolation with the stencil whose centre point is the closest to the departure one.

DOI: 10.1002/fld

Additional terms appear in the first equation and are enclosed in brackets with coefficient α in order to clarify their influence on the accuracy and stability in the following analysis. Such kind of modification of SC method was proposed and analysed by Douglas and Kim [19] and Douglas *et al.* [20] for solution of one parabolic equation. We extend their method to the case of hyperbolic system and apply it in the semi-Lagrangian scheme.

Evidently, Equations (8) represent explicit, weakly unstable step (without additional terms, this is the Euler forward scheme considered along trajectories). Stability is recovered by applying two corrections (9) and (10) in x- and y-direction, respectively. Solution of the explicit step equations does not require any discussion. Equations (9) are reduced to 1D difference elliptic equation

$$\begin{gathered}\Phi^{n+1,2} - \frac{\tau^2}{4}\Phi_0\delta_{x\Phi}\delta_{xV}\Phi^{n+1,2} = F \\ F = \Phi^{n+1,1} - \frac{\tau}{2}\Phi_0\delta_{x\Phi}\left[u^{n+1,1} - u^n + \frac{\tau f}{2}(v^{n+1,1} - v^n) + \frac{\tau}{2}\delta_{xV}\Phi^n\right]\end{gathered} \tag{11}$$

The second-order differences are calculated by

$$\delta_{x\Phi}\delta_{xV}\Phi^{n+1,2} = \frac{(\Phi_{i+1,j} - 2\Phi_{i,j} + \Phi_{i-1,j})^{n+1,2}}{h^2}$$

for jth row and

$$\delta_{x\Phi}\delta_{xV}\Phi^{n+1,2} = \frac{(\Phi_{i+3/2,j+1/2} - 2\Phi_{i+1/2,j+1/2} + \Phi_{i-1/2,j+1/2})^{n+1,2}}{h^2}$$

for $j+1/2$th row (see Figure 1). For each fixed value of y_j, Equations (11) completed with boundary conditions represent closed tridiagonal linear system, which is solved by applying efficient Thomas algorithm [22]. Stability of this algorithm is guaranteed by diagonal dominance of the system matrix. After finding $\Phi^{n+1,2}$, the values of $u^{n+1,2}$ and $v^{n+1,2}$ are calculated by explicit formulas in (9). System (10) is solved by exactly analogous method.

It is easy to show that the required boundary conditions for intermediate values can be defined with the second-order accuracy in the following simple form:

$$u^{n+1,1} = u^{n+1,2} = u^{n+1}, \quad v^{n+1,1} = v^{n+1,2} = v^{n+1}, \quad \Phi^{n+1,1} = \Phi^{n+1,2} = \Phi^{n+1} \tag{12}$$

on the set of boundary grid points. The formulation of the second-order accuracy and stable boundary conditions for elliptic equations (11) and their counterparts deduced for system (10) is slightly more sophisticated and should follow the discretized systems (9) and (10) rather than their differential prototypes. For example, considering system (9) for jth row (see Figure 1) with the boundary values $\Phi_{1,j}^{n+1,2}$, $u_{3/2,j}^{n+1,2}$, $\Phi_{I,j}^{n+1,2}$, $u_{I+1/2,j}^{n+1,2}$ specified by formulas (12), we obtain Equations (11) for indices $i = 2, \ldots, I-1$. These equations should be completed by two boundary conditions, first of which has the simple form

$$\Phi_{I,j}^{n+1,2} = \Phi_{I,j}^{n+1}$$

but the second is deduced from equations in (9) considered for $i = 2$ and boundary condition $u_{3/2,j}^{n+1,2} = u_{3/2,j}^{n+1}$ resulting in a more complex relation in the form

$$\Phi_{2,j}^{n+1,2} - \frac{\tau^2}{4}\Phi_0\frac{\Phi_{3,j}^{n+1,2} - \Phi_{2,j}^{n+1,2}}{h^2} = F_{2,j}$$

DOI: 10.1002/fld

$$F_{2,j}=\Phi_{2,j}^{n+1,1}-\frac{\tau}{2}\Phi_0\left[\frac{u_{5/2,j}^{n+1,1}-u_{3/2,j}^{n+1}}{h}-\frac{u_{5/2,j}^{n}-u_{3/2,j}^{n}}{h}+\frac{\tau f}{2}\frac{v_{5/2,j}^{n+1,1}-v_{5/2,j}^{n}}{h}+\frac{\tau}{2}\frac{\Phi_{3,j}^{n}-\Phi_{2,j}^{n}}{h^2}\right]$$

The use of more simple second boundary condition $\Phi_{I,j}^{n+1,2}=\Phi_{I,j}^{n+1}$, which seems to be natural at glance, leads to unstable scheme. Analogous boundary conditions are used for Equation (11) at $j+1/2$th row and for elliptic equation obtained from (10).

Thus, one time step consists of solution for trajectory equations (3)–(5) followed by algorithm (8)–(10) for adjustment part, which in its turn is separated in three substeps, the first of which is solved by explicit formulas (8) and the two last are reduced to solution of 1D difference elliptic equations with appropriate boundary conditions.

3. ANALYSIS OF ACCURACY AND STABILITY

Applying some algebra we can eliminate the intermediate values from (8)–(10) and obtain the following equations for the principal unknown functions:

$$\begin{aligned}\frac{u^{n+1}-u^n}{\tau}&=f\frac{v^{n+1}+v^n}{2}-\delta_{xV}\frac{\Phi^{n+1}+\Phi^n}{2}\\&\quad+\left[\frac{\tau f^2}{4}(u^{n+1}-u^n)+\frac{\tau f}{4}\delta_{yV}(\Phi^{n+1}-\Phi^n)-\frac{\tau\Phi_0}{4}\delta_{xV}\delta_{y\Phi}(v^{n+1}-v^n)\right]\\&\quad-\alpha\left[\frac{\tau f^2}{4}(u^n-u^{n-1})+\frac{\tau f}{4}\delta_{yV}(\Phi^n-\Phi^{n-1})-\frac{\tau\Phi_0}{4}\delta_{xV}\delta_{y\Phi}(v^n-v^{n-1})\right]\end{aligned}\tag{13}$$

$$\frac{v^{n+1}-v^n}{\tau}=-f\frac{u^{n+1}+u^n}{2}-\delta_{yV}\frac{\Phi^{n+1}+\Phi^n}{2}\tag{14}$$

$$\frac{\Phi^{n+1}-\Phi^n}{\tau}=-\Phi_0\left(\delta_{x\Phi}\frac{u^{n+1}+u^n}{2}+\delta_{y\Phi}\frac{v^{n+1}+v^n}{2}\right)-(\Phi^n-\Phi_0)(\delta_{x\Phi}u^n+\delta_{y\Phi}v^n)\tag{15}$$

Omitting the bracket terms in the first equation and substituting Φ for Φ_0 in the third equation, we obtain the second-order accuracy absolutely stable Crank–Nicholson scheme. The terms in the first bracket appear due to applied splitting technique, the second bracket contains additional terms of the Douglas modification and the last term in the third equation is the result of computation of corrections in (9) and (10) with constant divergence coefficient. Let us evaluate the influence of each of these terms on accuracy and stability of the scheme.

Evidently, Equation (13) is the second-order approximation to the first equation in (1) for arbitrary value of parameter α, (14) is the second-order approximation to the second equation in (1), and (15) is the second-order approximation to the third equation linearized about $\Phi=\Phi_0$. Therefore, (13)–(15) is the second-order approximation to (1), except for divergence term in the third equation, which is theoretically approximated with the first order of accuracy. However, if deviations from the mean geopotential Φ_0 are small, one can expect that the errors introduced by

DOI: 10.1002/fld

this linearization are small too. Indeed, the third equation in (1) can be rewritten in the equivalent form

$$\partial_t \ln \Phi + u\partial_x \ln \Phi + v\partial_y \ln \Phi = -(\partial_x u + \partial_y v)$$

Using corresponding approximations of this equations in (8)–(10)

$$\frac{\ln \Phi^{n+1,1} - \ln \Phi^n}{\tau} = -(\delta_{x\Phi} u^n + \delta_{y\Phi} v^n), \quad \frac{\ln \Phi^{n+1,2} - \ln \Phi^{n+1,1}}{\tau} = -\delta_{x\Phi} \frac{u^{n+1,2} - u^n}{2}$$

$$\frac{\ln \Phi^{n+1} - \ln \Phi^{n+1,2}}{\tau} = -\delta_{y\Phi} \frac{v^{n+1} - v^n}{2}$$

we can achieve the second order of accuracy for all system (1). However, there is a price for this theoretical improvement: elliptic equations for corrections become nonlinear. For example, equation for $\Phi^{n+1,2}$ assumes the form

$$\ln \Phi^{n+1,2} - \frac{\tau^2}{4} \delta_{x\Phi} \delta_{xV} \Phi^{n+1,2} = G$$

$$G = \ln \Phi^{n+1,1} - \frac{\tau}{2} \delta_{x\Phi} \left[u^{n+1,1} - u^n + \frac{\tau f}{2} (v^{n+1,1} - v^n) + \frac{\tau}{2} \delta_{xV} \Phi^n \right]$$

There is no problem in solving the last elliptic equation by iterative method such as Gauss–Seidel or successive overrelaxation (SOR), but the nonlinearity eliminates the possibility of applying more efficient direct Thomas algorithm. On the other hand, the numerical solution provided by the 'logarithmic' version of the scheme is virtually identical to the solution of scheme (8)–(10) as applied to forecasting the pressure level of the middle troposphere with the characteristic value $\Phi_0 \approx 5500\,\mathrm{m}$ and deviations about 5% of the mean value. Thus, since the linearized versions of the third equation in (9)–(10) admit more efficient numerical solution of elliptic problem, we have chosen these approximations.

Coefficient α in (8) is chosen to equal 1 in order to reduce the splitting errors. Indeed, in this case, the terms in two brackets form the approximations to the second-order time derivative

$$\phi^{n+1} - 2\phi^n + \phi^{n-1}, \quad \phi = u, v, \Phi$$

and consequently all bracket terms give an additional error of the third order. Since the second-time derivatives are sufficiently small in atmospheric motions of the large scale, the Douglas modification allows to reduce the negative effect of the splitting on overall accuracy for great time steps. The price for this improvement of approximation is very modest: one should calculate additional three terms in explicit form, which takes about 5% of the computational time of the traditional splitting scheme without α terms. Thus, we can conclude that the proposed scheme is practically of the second order of accuracy with the splitting errors of the third order.

Let us turn our attention to the analysis of stability of scheme (8)–(10). The advective part is solved by traditional algorithm and its stability criterion is given by (6). Let us investigate the linear stability of the adjustment step. Considering the primitive equations linearized about a state of the rest on an f-plane, we obtain (13)–(15) with zero trajectories (all values are defined at the grid points), $f = f_0$ in the first and second equations, and $\Phi = \Phi_0$ in the third equation,

DOI: 10.1002/fld

that is,

$$\frac{u^{n+1}-u^n}{\tau}=f_0\frac{v^{n+1}+v^n}{2}-\delta_{xV}\frac{\Phi^{n+1}+\Phi^n}{2}$$
$$+\left[\frac{\tau f_0^2}{4}(u^{n+1}-u^n)+\frac{\tau f_0}{4}\delta_{yV}(\Phi^{n+1}-\Phi^n)-\frac{\tau\Phi_0}{4}\delta_{xV}\delta_{y\Phi}(v^{n+1}-v^n)\right]$$
$$-\alpha\left[\frac{\tau f_0^2}{4}(u^n-u^{n-1})+\frac{\tau f_0}{4}\delta_{yV}(\Phi^n-\Phi^{n-1})-\frac{\tau\Phi_0}{4}\delta_{xV}\delta_{y\Phi}(v^n-v^{n-1})\right] \tag{16}$$

$$\frac{v^{n+1}-v^n}{\tau}=-f_0\frac{u^{n+1}+u^n}{2}-\delta_{yV}\frac{\Phi^{n+1}+\Phi^n}{2} \tag{17}$$

$$\frac{\Phi^{n+1}-\Phi^n}{\tau}=-\Phi_0\left(\delta_{x\Phi}\frac{u^{n+1}+u^n}{2}+\delta_{y\Phi}\frac{v^{n+1}+v^n}{2}\right) \tag{18}$$

Applying von Neumann spectral analysis, that is, substituting the representation of the difference solution in the form of a separate discrete wave in (16)–(18), we obtain the following characteristic equation:

$$(\lambda-1)P(\lambda)=0,\quad P(\lambda)=\lambda(\lambda-1)^2+A\lambda(\lambda+1)^2-B(\lambda-1)^2(\lambda-\alpha)+C(\lambda+1)^2(\lambda-\alpha) \tag{19}$$

$$A=\frac{\tau^2\Phi_0}{h^2}\left(\sin^2\frac{kh}{2}+\sin^2\frac{mh}{2}\right)+\frac{\tau^2 f_0^2}{4},\quad B=\frac{\tau^2 f_0^2}{4},\quad C=\frac{\tau^4\Phi_0^2}{h^4}\sin^2\frac{kh}{2}\sin^2\frac{mh}{2}$$

where λ is the amplification factor of the scheme and k and m are the wave numbers.

For the scheme to be stable, all the amplification factors should lie within the unit circle or on its boundary (in the last case, the amplification factor should be a simple root of characteristic equation). Evidently, $\lambda=1$ is the stable root and the others are defined from third-order polynomial equation $P(\lambda)=0$. In the case $\alpha=0$ (non-modified splitting), $\lambda=0$ is one more root (ϕ^{n-1} terms disappear from Equation (16)) and the remaining roots satisfy equation

$$(1-B)(\lambda-1)^2+(A+C)(\lambda+1)^2=0$$

These roots are stable iff

$$\left|\frac{A+C-(1-B)}{A+C+(1-B)}\right|\leqslant 1$$

that is,

$$\tau^2 f_0^2\leqslant 4$$

If $\alpha\neq 0$ the situation is more complex. To analyse the location of the roots in this case, we use one-to-one mapping

$$z=\frac{\lambda+1}{\lambda-1}$$

DOI: 10.1002/fld

from the unit circle onto the left half-plane of the extended complex plane. This way, equation $P(\lambda)=0$ is transformed to

$$P(z)=\tilde{A}z^3+\tilde{B}z^2+\tilde{C}z+\tilde{D}=(z+1)+Az^2(z+1)-B+2Cz^2=0 \tag{20}$$

According to the Lienard–Chipart criterion, the polynomial $P(z)$ has roots in the left half-plane iff all the coefficients $\tilde{A}, \tilde{B}, \tilde{C}, \tilde{D}$ are positive and the determinant $\Delta=\tilde{B}\tilde{C}-\tilde{A}\tilde{D}$ is positive too [28]. We confine analysis of (20) to the most important case $\alpha \in (0, 1]$. Then, elementary algebra shows that the above conditions are satisfied iff

$$\tau^2 f_0^2(1+\alpha)\leqslant 4 \tag{21}$$

For the maximum value $|f|_{\max}=1.4\times 10^{-4}\,\mathrm{s}^{-1}$ and $\alpha=1$ (modified splitting) we get $\tau \approx 160\,\mathrm{min}$, which is a very weak restriction. For example, in atmosphere and ocean modelling a greater time step is hard to be used.

4. NUMERICAL EXPERIMENTS

In order to evaluate the accuracy and efficiency of the method described in Section 2, we ran a series of numerical experiments over a square domain of side 5000 km centred at Porto Alegre city (30°S, 52°W), using oblique stereographic projection for representation of the Earth surface. This domain was covered by staggered E grid with mesh size $h=50\,\mathrm{km}$. The initial and boundary value conditions for geopotential height and wind components on the 500 hPa pressure surface were obtained from the objective analysis and global forecasts of the National Centers for Environmental Prediction (NCEP). In principle, a two-time-level scheme does not require special first step needed for three-time-level methods. However, special treatment should be given for the extrapolation formulas of wind (4) at the first advective step and for formulas (5) at the first and second steps. We assume $u^{1/2}=u^0$, $v^{1/2}=v^0$ in (4), (5) at the first time step and use (4) instead of (5) at the second time step.

A number of 24-h forecasts of the geopotential and wind fields were calculated using proposed modified splitting scheme ($\alpha=1$) with trajectories evaluated by formulas (3), (4) (MSL1) and (3), (5) (MSL2). Also non-modified version of the splitting algorithm ($\alpha=0$) with trajectories (3), (4) (SL1) and (3), (5) (SL2) and the Eulerian forward–backward (FB) scheme were run. The 'control' forecast by the FB scheme was run with the small time step $\tau=2\,\mathrm{min}$ corresponding to the CFL stability condition. In order to investigate the growth of the time truncation error as a function of the time step length, two semi-Lagrangian splitting schemes were run with different time steps. The accuracy of each integration was measured by comparing the forecasts with the corresponding 'control' results. The root-mean-square (RMS) differences between height forecasts are shown in Table I, where τ is the time step of integrations (in minutes), the shown numbers are RMS height differences between 24-h forecasts of chosen scheme and FB scheme (in metres), and $T_{\tau=60}$ is the central processing unit (CPU) time of one forecast with $\tau=60\,\mathrm{min}$ (in fractions of FB forecast time). The modified technique improves essentially the accuracy of the forecasts for time steps greater than 30 min. Taking into account that the computational cost of one forecast using SC scheme is proportional to τ^{-1}, we can conclude that the MSL1 and MSL2 schemes are certainly more efficient than SL1 and SL2. Although reducing of the splitting error is not sufficient for the largest time steps, the scheme remains stable up to $\tau=120\,\mathrm{min}$.

DOI: 10.1002/fld

Table I. RMS differences between tested (MSL1, MSL2, SL1, SL2, USL1 and USL2) schemes and reference (FB) scheme.

Scheme	$\tau = 10$	$\tau = 30$	$\tau = 60$	$\tau = 90$	$T_{\tau=60}$
MSL1	2.1	2.6	4.2	19.8	0.18
MSL2	2.0	2.5	3.9	18.3	0.18
SL1	2.2	3.8	26.4	67.5	0.17
SL2	2.1	3.6	25.7	66.1	0.17
USL1	2.0	2.5	3.7	6.8	0.24
USL2	2.0	2.5	3.7	6.8	0.32

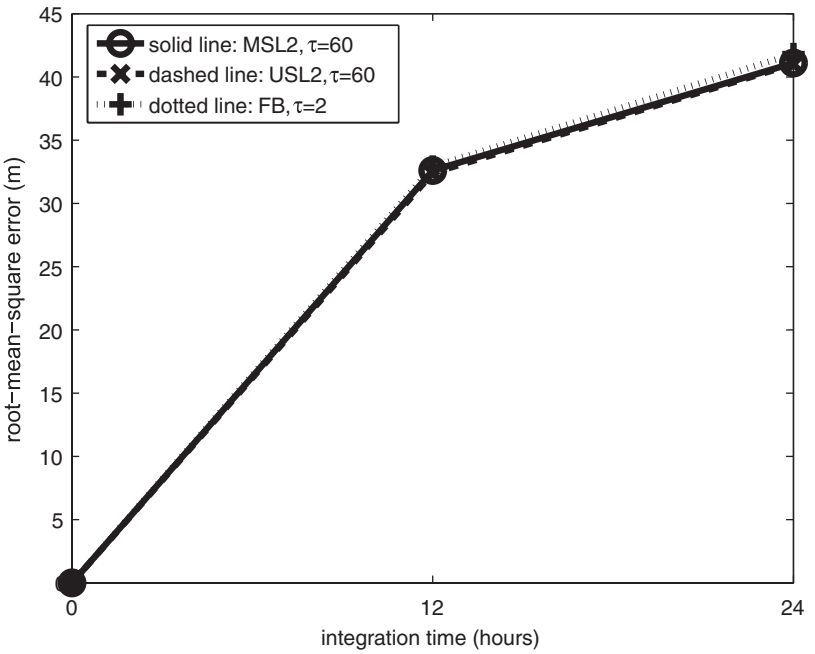

Figure 2. RMS errors of 24-h forecasts for three tested schemes: height field.

To provide a comparison of the performance between developed scheme and standard unsplit semi-implicit semi-Lagrangian scheme, we performed some experiments with unsplit version of the scheme. The last scheme is based on the same spatial discretization outlined in Section 2.1 and includes the same trajectory calculation algorithm described in Section 2.2. The adjustment step consists of implicit Crank–Nicholson approximation of (7) along the trajectories of particles. The details of approximation can be found in [27] with the only difference related to the Coriolis term. It was found to be suitable to present the Coriolis parameter as a sum of its mean value and deviations, and approximate the former term implicitly in Crank–Nicholson form and the latter term explicitly. This kind of approximation allows to simplify the elliptic equation for the implicit terms to the form of constant coefficient Helmholtz equation, and still keeps the same stability and accuracy as fully implicit approximation [29, 30]. The obtained 2D Helmholtz equation for the geopotential height

DOI: 10.1002/fld

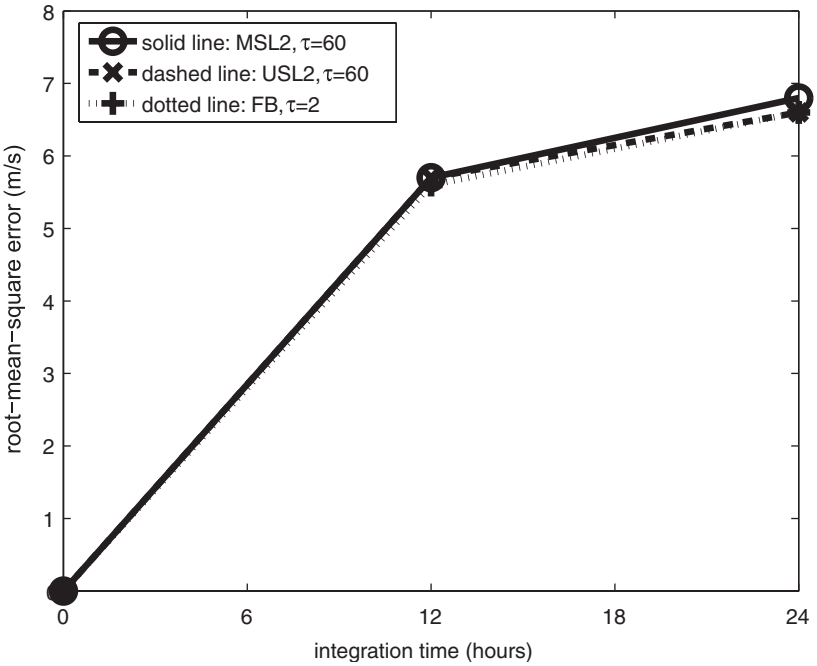

Figure 3. RMS errors of 24-h forecasts for three tested schemes: wind field.

can be solved by traditional SOR method or more efficient multigrid solvers, which have reliable implementations for this kind of problems. We applied the free available BOXMG solver, which allows the use of the rectangular grids with arbitrary number of the grid points [31, 32]. Through numerical experiments the most efficient versions of the point SOR method and BOXMG method were selected. For the SOR algorithm, the red–black ordering appeared to be about 1.5 times faster than lexicographic one. The optimal parameters of the BOXMG solver were defined as follows: the V-type cycle with application of two cycles, one four-colour Gauss–Seidel point relaxation sweep on any grid (except for the finest one) both before dropping down to the next coarser grid and before interpolation to the previous finer grid, two red–black point relaxation sweeps on the finest grid. The geopotential height of the current time level was used as initial guess for both methods. Under the above configurations, the BOXMG was about two times faster than SOR. In order to be sure that applied MG algorithm is sufficiently optimal, we compared it with the classic Brandt algorithm [33], which is designed especially for Poisson and Helmholtz problems with constant coefficients. The computational results for both MG algorithms are virtually identical on the spatial grid of 97×97 points (which is needed for double coarsening algorithm by Brandt in order to reach rather coarse grids) that leads us to believe that selected set of parameters for the BOXMG solver is rather optimal. The main advantage of the BOXMG solver in the context of our model is that it has equally good performance for the grids with arbitrary number of the points. Let us note that the separate solution of the adjustment equations by the modified SC scheme (8)–(10) is almost four times faster as compared with unsplit BOXMG algorithm. Thus, although theoretically both approaches are efficient solvers requiring $O(NM)$ operations for spatial grid with $N \times M$ points,

DOI: 10.1002/fld

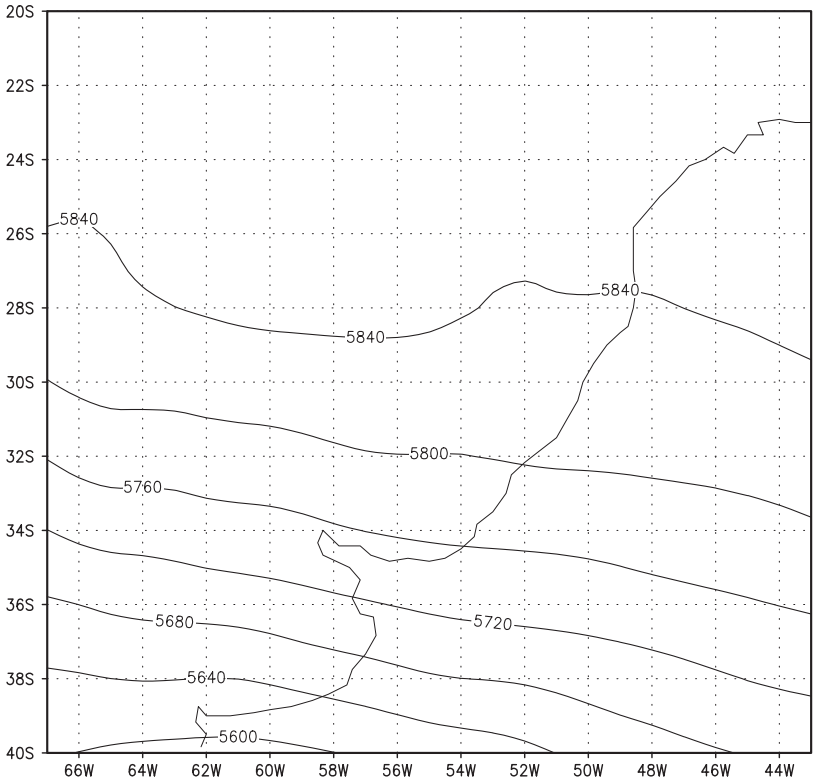

Figure 4. 500 hPa height field from NCEP analysis for 0000 UTC 30 November 2005.

the practical computational time is quite different. The results of the experiments with unsplit semi-Lagrangian method using SOR (USL1) and BOXMG (USL2) solvers are presented in the last two rows of Table I. One can see that MSL1 and MSL2 algorithms are more computationally efficient for time step $\tau = 60$ min even compared with the available optimal implementation of the unsplit version: the forecast differences are at the same level and the CPU time is notably better for splitting algorithms.

The objective evaluation of the accuracy of the predicted geopotential and wind fields at 500 hPa pressure surface was performed by computing the RMS differences between 24-h forecasts and the NCEP analysis. The results for MSL2 (with $\tau = 60$ min), USL2 (with $\tau = 60$ min) and FB (with $\tau = 2$ min) schemes are shown in Figures 2 and 3 for height and wind fields, respectively. Overall values of this measure of forecast skill are quite characteristic for the SW model [34].

To access qualitative synoptic evaluation of the MSL2 scheme performance, we show the height charts for two 24-h forecasts in the inner evaluation window of the prognostic domain. Figures 4–11 contain two sequences of the charts: two charts of the analysis fields (at the initial instant and 24 h later), as well the charts of the 24-h forecasts performed by FB and MSL2 schemes. One can see that the forecast quality is good for both schemes in the first case (Figures 4–7) when large-scale atmospheric dynamics is determined primarily by advective processes. The standard

DOI: 10.1002/fld

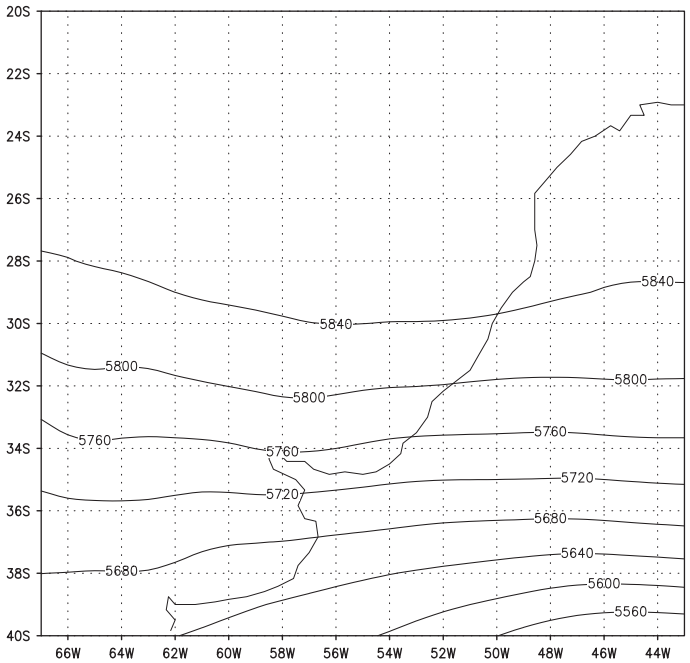

Figure 5. 500 hPa height field from NCEP analysis for 0000 UTC 01 December 2005.

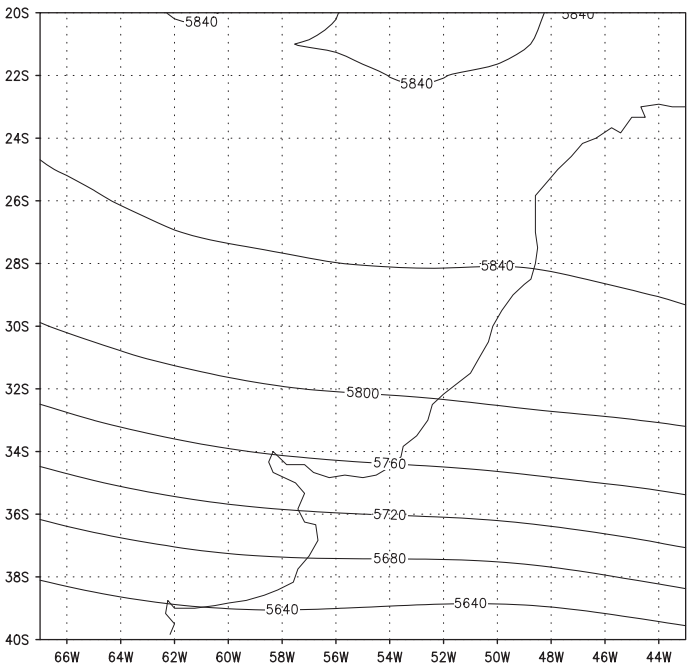

Figure 6. 24-h FB forecast of 500 hPa height field for 0000 UTC 01 December 2005.

DOI: 10.1002/fld

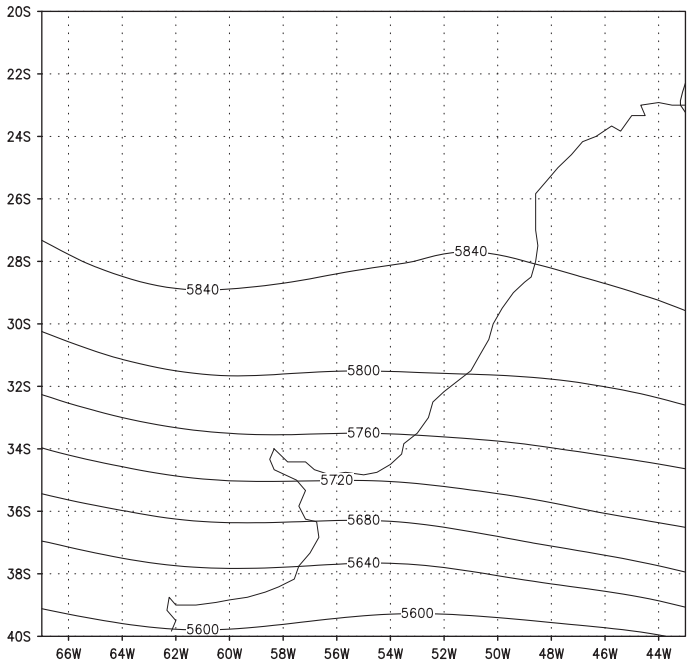

Figure 7. 24-h MSL2 forecast of 500 hPa height field for 0000 UTC 01 December 2005.

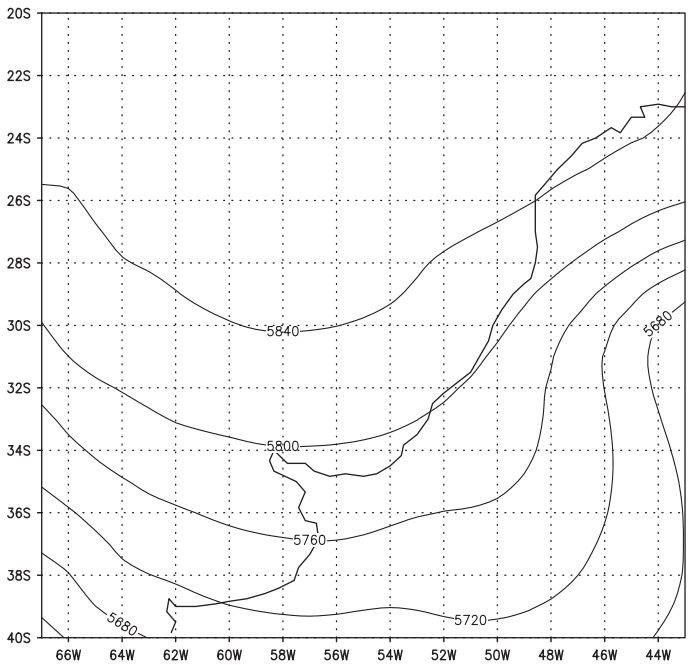

Figure 8. 500 hPa height field from NCEP analysis for 0000 UTC 03 December 2005.

DOI: 10.1002/fld

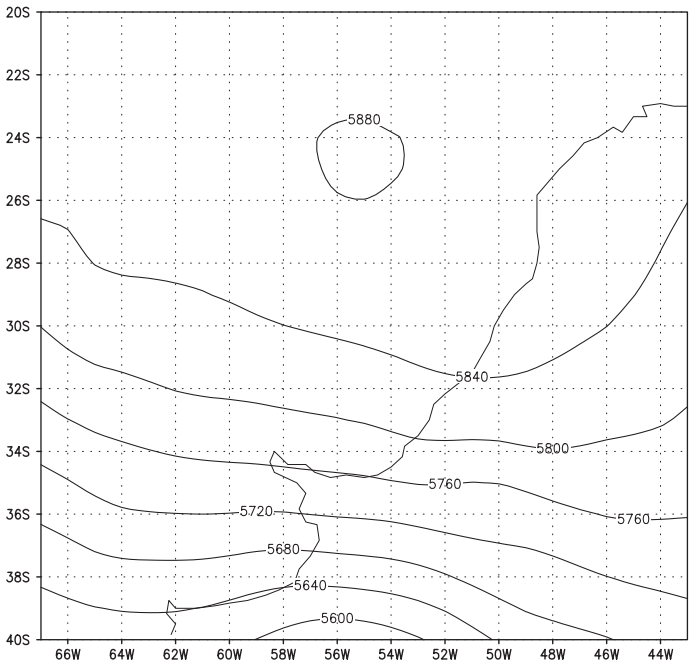

Figure 9. 500 hPa height field from NCEP analysis for 0000 UTC 04 December 2005.

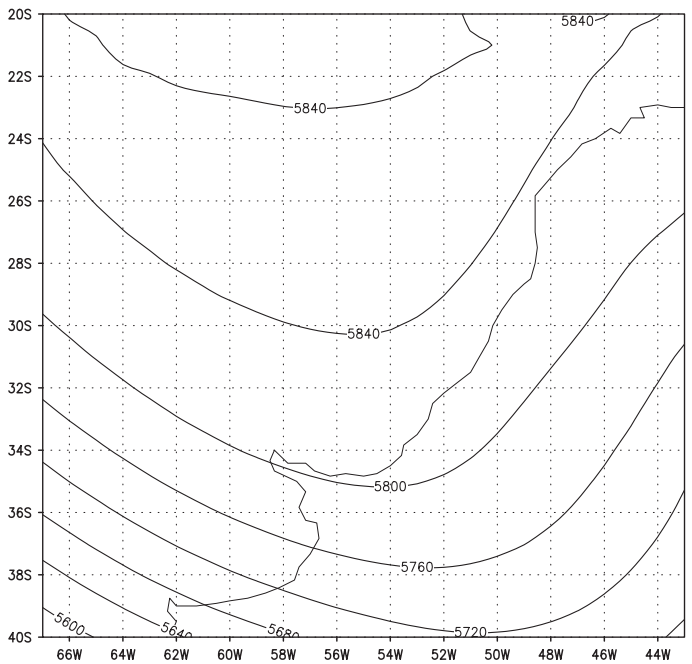

Figure 10. 24-h FB forecast of 500 hPa height field for 0000 UTC 04 December 2005.

DOI: 10.1002/fld

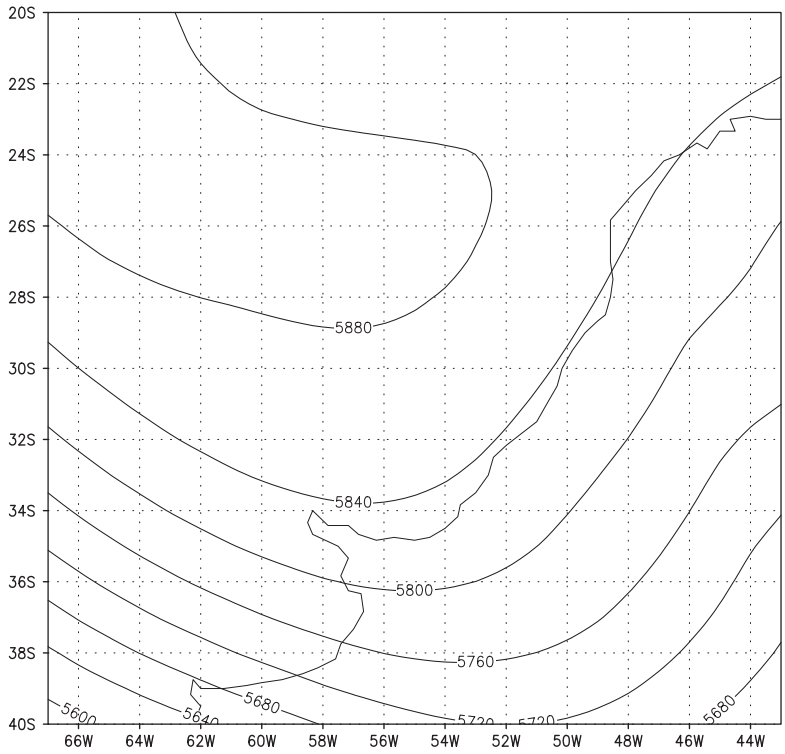

Figure 11. 24-h MSL2 forecast of 500 hPa height field for 0000 UTC 04 December 2005.

statistical evaluations [34] confirm that this forecast is rather successful for both schemes: the RMS error for FB and MSL2 schemes is 41.1 and 32.6 m, and the correlation coefficient between observed and predicted tendencies is 0.93 and 0.94, respectively.

In the second sequence of the charts, the development of the anticyclonic formation can be observed in real data (Figures 8 and 9). The forecast chart for the MSL2 scheme (Figure 11) shows that the scheme failures in capturing this formation, but so does the FB scheme (Figure 10), because this is characteristic case when the SW approximation does not work well [35, 36]. The statistical evaluations for this case are: the RMS error for FB and MSL2 schemes is 57.2 and 62.1 m, and the correlation coefficient between observed and predicted tendencies is 0.73 and 0.69, respectively.

Thus, the proposed algorithm has the important properties of efficient schemes: all principal components of the MSL1 and MSL2 schemes involve only efficient solvers with the number of arithmetic operations directly proportional to the number of points of spatial grid, these schemes are stable for great time steps, and they assure required level of accuracy compatible with more simple and less efficient schemes. Therefore, the proposed schemes are quite efficient for atmospheric and oceanographic problems where physical considerations require the use of time steps up to one hour, which is a common situation in limited area and mesoscale modelling.

DOI: 10.1002/fld

ACKNOWLEDGEMENT

This research was supported by Brazilian science foundation CNPq.

REFERENCES

1. Pudykiewicz J, Benoit R, Staniforth A. Preliminary results from a partial LRTAP model based on an existing meteorological forecast model. *Atmosphere-Ocean* 1985; **23**:267–303.
2. Staniforth A, Cote J. Semi-Lagrangian integration schemes for atmospheric models—a review. *Monthly Weather Review* 1991; **119**:2206–2223.
3. Benoit R, Desgagne M, Pellerin P, Pellerin S, Chartier Y, Desjardins S. The canadian MC2: a semi-Lagrangian, semi-implicit wideband atmospheric model suited for finescale process studies and simulation. *Monthly Weather Review* 1997; **125**:2382–2415.
4. Cote J, Gravel S, Methot A, Patoine A, Roch M, Staniforth A. The operational CMC-MRB global environmental multiscale (GEM) model. Part I: Design considerations and formulation. *Monthly Weather Review* 1998; **126**: 1373–1395.
5. Gospodinov IG, Spiridonov VG, Geleyn JF. Second-order accuracy of two-time-level semi-Lagrangian schemes. *Quarterly Journal of the Royal Meteorological Society* 2001; **127**:1017–1033.
6. Guo DX, Drake JB. A global semi-Lagrangian spectral model for the reformulated shallow water equations. *Discrete and Continuous Dynamical Systems* 2003; 375–385.
7. Guo DX, Drake JB. A global semi-Lagrangian spectral model of the shallow water equations with variable resolution. *Journal of Computational Physics* 2005; **206**:559–577.
8. Hortal M. The development and testing of a new two-time-level semi-Lagrangian scheme (SETTLS) in the ECMWF forecast model. *Quarterly Journal of the Royal Meteorological Society* 2002; **128**:1671–1687.
9. Kiehl JT, Hack JJ, Bonan GB, Boville BA, Williamson DL, Rasch PJ. The national center for atmospheric research community climate model: CCM3. *Journal of Climate* 1998; **11**:1131–1149.
10. Ritchie H, Temperton C, Simmons A, Hortal M, Davies T, Dent D, Hamrud M. Implementation of the semi-Lagrangian method in a high-resolution version of the ECMWF forecast model. *Monthly Weather Review* 1995; **123**:489–514.
11. Behrens J. Atmospheric and ocean modeling with an adaptive finite element solver for the shallow-water equations. *Applied Numerical Mathematics* 1998; **26**:217–226.
12. Hannert E, LeRoux DY, Legat V, Deleersnijder E. An efficient Eulerian finite element method for the shallow water equations. *Ocean Modelling* 2005; **10**:115–136.
13. LeRoux DY, Lin CA, Staniforth A. A semi-implicit semi-Lagrangian finite-element shallow-water ocean model. *Monthly Weather Review* 2000; **128**:1384–1401.
14. Bates JR. An efficient semi-Lagrangian and alternating direction implicit method for integrating the shallow water equations. *Monthly Weather Review* 1984; **112**:2033–2047.
15. Cohn SE, Dee D, Isaacson E, Marchesin D, Zwas G. A fully implicit scheme for the barotropic primitive equations. *Monthly Weather Review* 1985; **113**:436–448.
16. Kar SK, Turco RP, Mechoso CR, Arakawa A. A locally one-dimensional semi-implicit scheme for global gridpoint shallow-water models. *Monthly Weather Review* 1994; **122**:205–222.
17. Wicker LJ, Skamarock WC. Time-splitting methods for elastic models using forward time schemes. *Monthly Weather Review* 2002; **130**:2088–2097.
18. Yakimiw E, Robert A. Accuracy and stability analysis of a fully implicit scheme for the shallow water equations. *Monthly Weather Review* 1986; **114**:240–244.
19. Douglas J, Kim S. Improved accuracy for locally one-dimensional methods for parabolic equations. *Mathematical Models and Methods in Applied Sciences* 2001; **11**:1563–1579.
20. Douglas J, Kim S, Lim H. An improved alternating-direction method for a viscous wave equation. *Current Trends in Scientific Computing*, *Contemporary Mathematics* 2003; **329**:99–104.
21. Vreugdenhil CB. *Numerical Methods for Shallow Water Flow*. Kluwer: Dordrecht, 1994.
22. Wesseling P. *Principles of Computational Fluid Dynamics*. Springer: Berlin, 2001.
23. Janjic Z, Mesinger F. Response to small-scale forcing on two staggered grids used in finite-difference models of the atmosphere. *Quarterly Journal of the Royal Meteorological Society* 1989; **115**:1167–1176.
24. Mesinger F, Arakawa A. *Numerical Methods Used in Atmospheric Models*. GARP Publishing Series: Geneva, 1976.

DOI: 10.1002/fld

25. Randall DA. Geostrophic adjustment and the finite-difference shallow-water equations. *Monthly Weather Review* 1994; **115**:1446–1450.
26. Robert A, Yee TL, Ritchie H. A semi-Lagrangian and semi-implicit numerical integration scheme for multilevel atmospheric models. *Monthly Weather Review* 1985; **113**:388–394.
27. Temperton C, Staniforth A. An efficient two-time-level semi-Lagrangian semi-implicit integration scheme. *Quarterly Journal of the Royal Meteorological Society* 1987; **113**:1025–1039.
28. Gantmacher FR. *The Theory of Matrices*. American Mathematical Society: New York, 1998.
29. Bourchtein A. Semi-Lagrangian scheme with multigrid solver. *Russian Meteorology and Hydrology* 1994; **5**:16–24.
30. McDonald A, Haugen J. A two-time-level, three-dimensional semi-Lagrangian, semi-implicit, limited-area gridpoint model of the primitive equations. *Monthly Weather Review* 1992; **120**:2603–2621.
31. Bandy V, Sweet R. A set of three drivers for BOXMG: a black box multigrid solver. *Communications in Applied Numerical Methods* 1992; **8**:563–571.
32. Dendy JE. Black box multigrid. *Journal of Computational Physics* 1982; **48**:366–386.
33. Brandt A. Multi-level adaptive solutions to boundary-value problems. *Mathematics of Computation* 1977; **31**: 333–390.
34. Anthes RA, Kuo YH, Hsie EY, Low-Nam S, Bettge TW. Estimation of skill and uncertainty in regional numerical models. *Quarterly Journal of the Royal Meteorological Society* 1989; **115**:763–806.
35. Holton JR. *An Introduction to Dynamic Meteorology*. Academic Press: San Diego, 2004.
36. Thompson PD. *Numerical Weather Analysis and Prediction*. MacMillan Co.: New York, 1961.

DOI: 10.1002/fld